Tuning electronic correlations in transition metal pnictides: Chemistry beyond the valence count

E. Razzoli,[1,2,*] C. E. Matt,[1,3] M. Kobayashi,[1,4] X.-P. Wang,[5] V. N. Strocov,[1] A. van Roekeghem,[5,6] S. Biermann,[6,7,8] N. C. Plumb,[1] M. Radovic,[1] T. Schmitt,[1] C. Capan,[9] Z. Fisk,[9] P. Richard,[5,10] H. Ding,[5,10] P. Aebi,[2] J. Mesot,[1,3,11] and M. Shi[1]

[1]*Swiss Light Source, Paul Scherrer Institute, CH-5232 Villigen PSI, Switzerland*
[2]*Département de Physique and Fribourg Center for Nanomaterials, Université de Fribourg, CH-1700 Fribourg, Switzerland*
[3]*Laboratory for Solid State Physics, ETH Zürich, CH-8093 Zürich, Switzerland*
[4]*Department of Applied Chemistry, School of Engineering, University of Tokyo, 7-3-1 Hongo, Bunkyo-ku, Tokyo 113-865 6, Japan*
[5]*Beijing National Laboratory for Condensed Matter Physics, and Institute of Physics, Chinese Academy of Sciences, Beijing 100190, China*
[6]*Centre de Physique Theorique, Ecole Polytechnique, CNRS, F-91128 Palaiseau Cedex, France*
[7]*Collège de France, 11 place Marcelin Berthelot, F-75005 Paris, France*
[8]*European Theoretical Synchrotron Facility, Europe*
[9]*Department of Physics and Astronomy, University of California Irvine, Irvine, California 92697, USA*
[10]*Collaborative Innovation Center of Quantum Matter, Beijing, China*
[11]*Institut de la Matiere Complexe, EPF Lausanne, CH-1015 Lausanne, Switzerland*

(Received 6 February 2015; revised manuscript received 15 May 2015; published 3 June 2015)

The effects of electron-electron correlations on the low-energy electronic structure and their relationship with unconventional superconductivity are central aspects in the research on iron-based pnictide superconductors. Here we use soft x-ray angle-resolved photoemission spectroscopy to study how electronic correlations evolve in different chemically substituted iron pnictides. We find that correlations are intrinsically related to the effective filling of the correlated orbitals, rather than to the filling obtained by valence counting. Combined density functional theory and dynamical mean-field theory calculations capture these effects, reproducing the experimentally observed trend in the correlation strength. The occupation-driven trend in the electronic correlation reported in our paper supports and extends the recently proposed connection between cuprate and pnictide phase diagrams.

DOI: 10.1103/PhysRevB.91.214502 PACS number(s): 74.70.Xa, 74.25.Jb

I. INTRODUCTION

Many recent studies have focused on the importance of the occupancy of the bands close to the Fermi level (E_F) in promoting the superconducting state of iron-based superconducting pnictides [1,2]. Most interestingly, when the filling is expressed with respect to the half-filled $3d^5$ bands, a striking similarity of the iron pnictide phase diagram to that of high-temperature superconducting cuprates has been pointed out [1,3], suggesting links between strongly correlated Mott insulating behavior and unconventional superconductivity. In iron pnictides, electronic Coulomb correlations are largely driven by Hund's exchange coupling [4–6], leading to a strong dependence even of the normal state properties on doping [7] and possible orbital selectivity in the strong coupling regime [8]. Theoretical models including the fivefold orbital manifold and Hund's rule coupling in addition to local Hubbard interactions [9,10] reproduce the main consequences of the change of filling induced by doping, in particular, a regime with strongly enhanced effective masses when approaching the d^5 configuration, even at local Hubbard interactions much smaller than the critical one. However, while this picture works well in the case of substitution of Ba with K or of Fe with Co [11], it fails in the case of isovalent substitution, e.g., for $BaFe_2As_{2-x}P_x$, where the correlations change with x but the nominal filling of the correlated bands does not [2]. Quite generally, the link between the correlation strength in the Fe pnictides and the valence count remains elusive.

In this paper, we emphasize the conceptual difference between the nominal valence count corresponding to the band filling and the effective orbital occupancies of the correlated states. Based on a combined experimental and theoretical spectroscopic study, we show that the latter is a more reliable tuning parameter for electronic correlations. We perform soft x-ray angle-resolved photoemission spectroscopy (SX-ARPES) for a series of stoichiometric 122 pnictides, namely, $LaFe_2P_2$, $CaFe_2P_2$, and $BaFe_2As_2$. The use of SX-ARPES, with its increased probing depth compared to ARPES performed with ultraviolet light as the excitation source (UV-ARPES), is essential for the determination of the bulk electronic structure of these materials since it has been demonstrated that they show a surface state when measured in the UV range [12–14]. Moreover, we combine the SX-ARPES results with combined density functional theory and dynamical mean-field theory (DFT+DMFT) calculations to show how the electronic correlation effects are associated with the detailed electronic structure and filling in the studied series of stoichiometric 122 pnictides. In particular, when d-orbital occupations are considered rather than nominal chemical valences, a clear link between the evolution of the strength of electronic correlations and filling emerges. Indeed, contrarily to naive valence counting arguments, we find that the substitution of La with Ca does not change the d-orbital occupation, whereas the seemingly isovalent substitution of As by P does. Furthermore, we identify the source of the latter change in the occupation, namely, the change in bonding (BB) antibonding splitting of the pnictogen atoms due to the isovalent substitution. Our results reveal that the changes in the correlation strength are mainly driven by unexpected changes in the orbital-resolved occupancy of the bands close to E_F, suggesting that such changes may be fundamental in determining the superconducting properties of a given compound.

*Corresponding author: elia.razzoli@unifr.ch

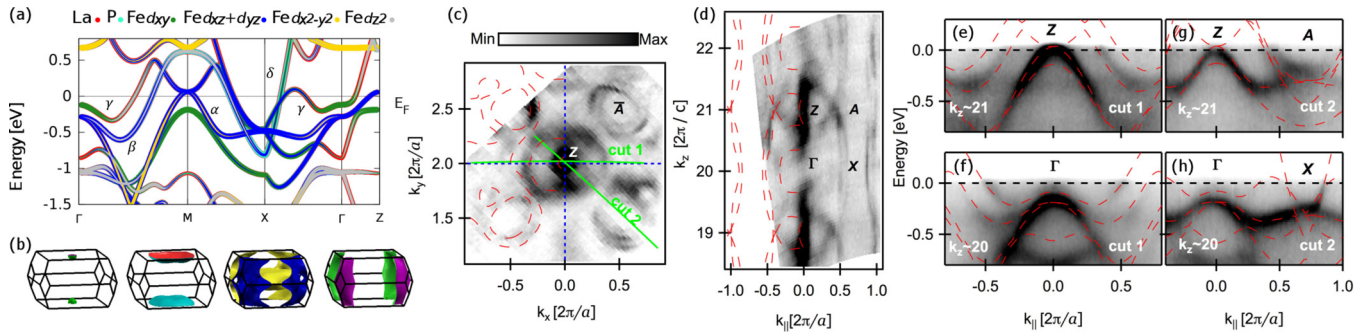

FIG. 1. (Color online) DFT band structure and SX-ARPES intensity maps of $LaFe_2P_2$. (a) Band structure along high symmetry lines. The thickness of the colored line is proportional to the corresponding character of the band. (b) Fermi surface plotted using XCRYSDEN visualization package [17]. (c) FS map with $h\nu = 575$ eV. The superimposed dashed lines are the DFT FS sheets. (d) FS map along cut 2 in (c), taken with $h\nu = 440$–640 eV in steps of 2.5 eV. The superimposed dashed lines in (c) and (d) are the FS from DFT calculations for $k_{\|} < 0$. (e), (f) ARPES spectra along cut 1 in (c) at $h\nu = 575$ and 525 eV, respectively. The cut at $h\nu = 575$ eV ($h\nu = 525$ eV) is close to the Z-Γ (Γ-M) direction. (g), (h) ARPES spectra along cut 2 in (c) at $k_z = 21$ and 20, respectively. The DFT bands are renormalized by a factor $(W_{\mathrm{DFT}}/W)_{\mathrm{ARPES}} = 1.5$.

II. EXPERIMENTAL DETAILS

The SX-ARPES experiments were performed at the Advanced Resonant Spectroscopies (ADRESS) beamline at the Swiss Light Source (SLS). The experimental geometry is described in Ref. [15]. Data were collected using circularly polarized light with an overall energy resolution of 50–80 meV. The samples were cleaved *in situ* at 11 K and measured in a vacuum always better than 5×10^{-11} mbar. The $\boldsymbol{k}$ values are determined by taking into account the photon momentum and are expressed in units of $(2\pi/a, 2\pi/a, 2\pi/c)$. The k_z values were extracted by using the free-electron final-state approximation with an inner potential $V_0 = 13$ for $LaFe_2P_2$ and $CaFe_2P_2$, and $V_0 = 14$ for $BaFe_2As_2$. All the intensity maps shown in the main text are obtained by integrating the ARPES spectral weight in an energy window of $E_F \pm 10$ meV.

III. EXPERIMENTAL RESULTS

Figure 1(a) shows the band structure of $LaFe_2P_2$ obtained using the WIEN2K software package [16]. The lattice constants used in the calculations are listed in Table I. The calculated Fermi surface (FS) [Fig. 1(b)] is similar to that of $LaRu_2P_2$ presented in Ref. [13] with the exception that there is an additional band (γ in Fig. 1) that crosses E_F along the Γ-X direction in $LaFe_2P_2$ and forms a small hole pocket at the zone corner. In Figs. 1(c) and 1(d) we plot the ARPES spectral weight mapping at E_F near the $(k_x, k_y, 21)$ and in the $(k_{\|}, 2-k_{\|}, k_z)$ plane. The k_z values were extracted by using the free-electron final-state approximation (FEFSA) [22]. The overlaid dashed lines show the FS from DFT calculations for $k_x < 0$ (the FS for $k_x > 0$ is obtained by reflection with respect to the $k_x = 0$ axis). The k_z variation as a function of (k_x, k_y) in the ARPES measurements with fixed photon energy has been taken into account according to the FEFSA. The observed FS is in good agreement with DFT calculations and it is highly three dimensional, similarly to the case of $LaRu_2P_2$ [13].

TABLE I. The lattice constants and internal atomic positions for $LaRu_2P_2$ [18], $LaFe_2P_2$ [19], $CaFe_2P_2$ [20], and $BaFe_2As_2$ [21].

Sample	a (Å)	c (Å)	z_{Pn}
$LaRu_2P_2$	4.031	10.675	0.3593
$LaFe_2P_2$	3.841	10.982	0.3554
$CaFe_2P_2$	3.855	9.985	0.3643
$BaFe_2As_2$	3.957	12.969	0.354

The ARPES intensity as a function of energy and k along cut 1 in Fig. 1(c) at $h\nu = 575$ eV ($k_z \sim 21$) and 525 eV ($k_z \sim 20$) are shown in Figs. 1(e) and 1(f), respectively. Since the value of k_z changes substantially along cut 2 in Fig. 1(c) ($\Delta k_z \sim 0.5$), to trace the band dispersion along the Γ-X and Z-A symmetry axes we made interpolations between spectra at different photon energies to obtain the spectra with constant k_z shown in Figs. 1(g) and 1(h). The DFT band structures (dashed lines) are superimposed on the data. Contrary to the case of $LaRu_2P_2$, where DFT reproduces the measured band dispersion quite well, the overall agreement between the ARPES spectra and the calculated electronic structure of $LaFe_2P_2$ becomes reasonable, for the bands close to E_F ($|E - E_F| \lesssim 0.6$ eV), only once the DFT bands are renormalized by a factor $(W_{\mathrm{DFT}}/W)_{\mathrm{ARPES}} = 1.5 \pm 0.1$ (red dashed lines). Assuming a purely local and orbital-independent many-body self-energy to be at the origin of this renormalization, we estimate a quasiparticle residue of $Z_{\mathrm{ARPES}} = 0.67 \pm 0.05$ [23]. All the bands close to the E_F are renormalized by this same factor, as evident from the curvature [24], energy distribution curve (EDC), and momentum distribution curve (MDC) analyses of Fig. 2.

The decrease of the bare bandwidth, due to the change in the principal quantum number of the electrons close to the E_F, as well as the increase of the Hubbard interaction U and Hund's coupling J (see Table II) upon isovalent substitution of Ru with Fe significantly contributes to the increasing correlations in the system. However, the observed band renormalization factor in $LaFe_2P_2$ is smaller than in the antiferromagnetic (AFM) compound (e.g., $BaFe_2As_2$) and in the superconducting 122 Fe-based pnictides (e.g., $Ba_{1-x}K_xFe_2As_2$), indicating that the above changes induced by the Ru $\rightarrow$ Fe substitution are not the only mechanisms responsible for the increase of the strength of the electronic correlations observed in these systems.

To investigate the effect of hole doping in the system, we performed a similar study for $CaFe_2P_2$, which has one

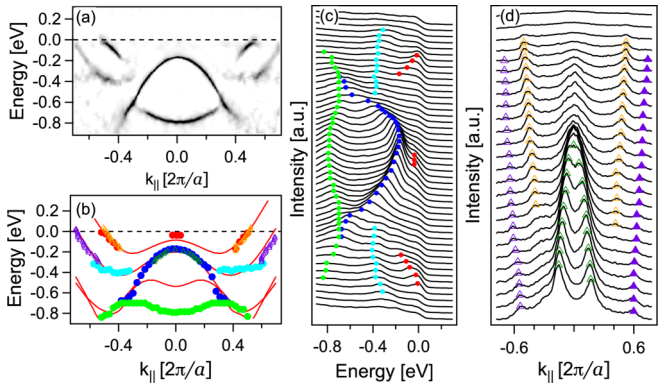

FIG. 2. (Color online) Curvature, EDC, and MDC analysis for the Γ-M direction. (a) Curvature intensity plot obtained from Fig. 1(f). (b) MDC and EDC peaks superimposed on the renormalized DFT bands. (c), (d) EDCs and MDCs from Fig. 1(f).

more hole per unit cell compared to $LaFe_2P_2$ and $LaRu_2P_2$. Similar to these compounds, the three-dimensional (3D) FS of $CaFe_2P_2$ is in good agreement with the DFT calculations [see Figs. 3(a)–3(d)], while the band structure has to be renormalized by a factor of $(W_{\mathrm{DFT}}/W)_{\mathrm{ARPES}} = 1.5 \pm 0.1$ [Figs. 3(e) and 3(f)]. This result is quite surprising, since the bandwidth renormalization is not influenced by the formal decrease in the number of the electrons due to the La to Ca substitution, contrary to the expected behavior of a system moving toward half filling [28]. However, this is explained once the multiband nature of these systems is taken into account. Comparison between Figs. 1(a) and 3(a) shows that the substitution of La with Ca does not result in a rigid shift of all the bands. Rather, only one band [γ in Fig. 1(a)] is fully pushed above E_F, while the others (with Fe d character) crossing E_F are qualitatively unchanged. This is mainly due to the fact that the γ band is very sensitive to the La to Ca substitution since it is essentially a La (Ca) band hybridizing (strongly in the case of La) with Fe d and P p states. The filling of the d bands is thus barely changed even if the total number of electrons in the unit cell is decreased by 1. We note here that the comparison between our finding and the mass enhancement measured by various quantum oscillation experiments (m/m_{DFT} in Table II) shows that while the electron-phonon interactions are responsible for the main contribution to the mass enhancement in $LaRu_2P_2$, most likely causing its low-T_c superconducting state, they are negligible in $LaFe_2P_2$ and $CaFe_2P_2$, which are indeed not superconducting.

Having discussed the role of the La to Ca substitution, it is now important to clarify the origin of the change in the bandwidth renormalization from $CaFe_2P_2$ to $BaFe_2As_2$. The nominal filling, the screened Coulomb interaction U, and the Hund's coupling J (see Table II) are very similar in the two systems, suggesting similarities in the electronic correlations. However, our measurements for $BaFe_2As_2$ (see Fig. 4), for which a similar analysis as above leads to identifying a bandwidth renormalization $\sim 2.1 \pm 0.2$ ($Z_{\mathrm{ARPES}} = 0.48 \pm 0.05$), in agreement with the existent ARPES measurements in the UV range [29], indicate that there is a sizable increase in the bandwidth renormalization. Again, the change in the bandwidth renormalization can be understood once the effective filling of the d bands is considered, instead of the nominal value. A first indication that the actual filling of the d bands is decreased in $BaFe_2As_2$ comes from comparing the DFT calculations. Focusing on the d_{xz} (d_{yz}) bands, the comparison between Figs. 3(a) and 4(a) reveals that the bands at -250 meV in $CaFe_2P_2$ are very similar to the ones at E_F in $BaFe_2As_2$, i.e., these bands appear shifted by 250 meV with respect to each other. The change in the band structure in this case is mainly due to the P to As substitution (similarly to the case of $CaFe_2P_2$ and $CaFe_2As_2$ [26]), which results in a change in the distance between the pnictide atoms Pn (Pn = P, As) of two adjacent Fe-Pn layers. In case of smaller distance (in $CaFe_2P_2$) the stronger bonding (BB) antibonding (AB) splitting of the Pn bands results in the AB bands being above E_F [in particular, the band at 0.5 eV at the X point in Fig. 3(a) [30]]. In the case of a larger distance, as in $BaFe_2As_2$, the splitting is smaller and the same band now crosses E_F. To compensate the increase of the carriers in this band, the other bands shift towards E_F. A clear demonstration of this mechanism is shown in Fig. 5(a), where the DFT calculations for $CaFe_2P_2$ are performed as a function of the P-P distance for a fixed P-Fe distance. We finally note that the transition from a three-dimensional (in $CaFe_2P_2$) into a more two-dimensional FS (in $BaFe_2As_2$), induced by the increase of the Pn-Pn distance, may also influence the change of the strength of the electronic correlations between the two systems.

To summarize, we have shown that while the weak strength of correlations in $LaRu_2P_2$ is mainly due to its larger bare bandwidth W_{DFT} [see Table II and Fig. 5(d)], the evolution of the correlation strength in $LaFe_2P_2$, $CaFe_2P_2$, and $BaFe_2As_2$ is driven by the effective filling of the d orbitals crossing the E_F. The strength of the correlations remains constant in $LaFe_2P_2$ and $CaFe_2P_2$ due to the similar filling, and increases in $BaFe_2As_2$ when the filling decreases [see Fig. 5(b)]. This result differs from what would be naively expected from the nominal

TABLE II. Critical temperature, ground state, bandwidth renormalization with respect to DFT extracted from ARPES, mass enhancements reported in the literature, Hubbard U and Hund's coupling J calculated from the constrained random phase approximation (cRPA), bare bandwidth obtained from DFT, vertical pnictogen-pnictogen distance, and nominal occupation of the 3d shell for the samples $LaRu_2P_2$, $LaFe_2P_2$, $CaFe_2P_2$, and $BaFe_2As_2$.

Sample	T_c (K)	Ground state	$\frac{W_{\mathrm{DFT}}}{W_{\mathrm{ARPES}}}$	$\frac{m}{m_{\mathrm{DFT}}}$	U_{cRPA} (eV)	J_{cRPA} (eV)	W_{DFT} (eV)	$z^{\perp}_{\mathrm{Pn\text{-}Pn}}$ (Å)	n_d^{nom}
$LaRu_2P_2$	4 [19]	Low T_c SC	1 [13]	2 [25]	1.89	0.502	9.4	3.00 [19]	6.5
$LaFe_2P_2$		Non-SC	1.5	1.8 [25]	2.035	0.695	7.55	3.20 [19]	6.5
$CaFe_2P_2$		Non-SC	1.5	1.5 [26]	2.632	0.723	7.50	2.71 [20]	6
$BaFe_2As_2$	142 [21]	AFM	2.1	2–3 [27]	2.572	0.78	7.4	3.78 [21]	6

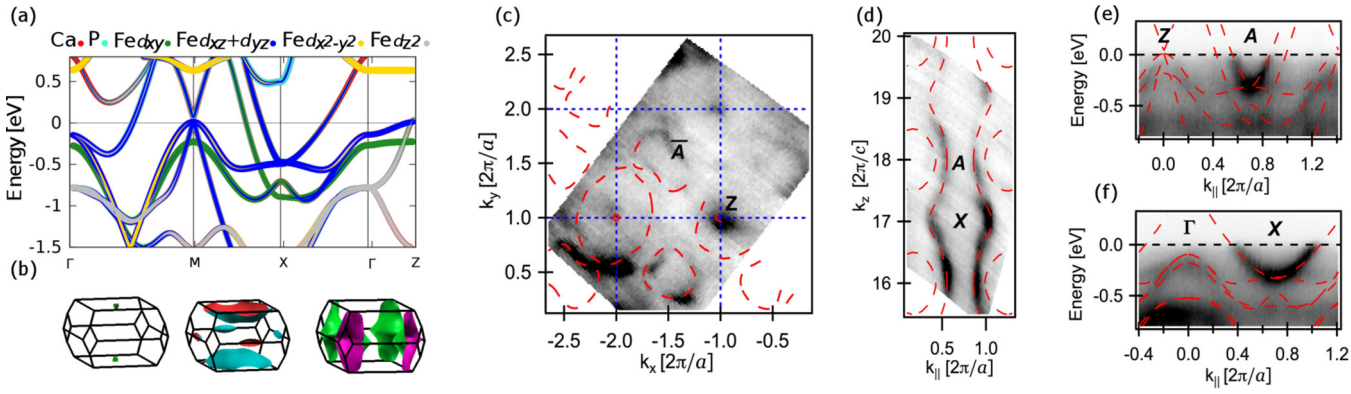

FIG. 3. (Color online) DFT band structure and SX-ARPES intensity maps of $CaFe_2P_2$. (a) Band structure along high symmetry lines. (b) Three-dimensional FS sheets of different bands. (c) FS map with $h\nu = 525$ eV. (d) Intensity maps in the $(k_\parallel - 2, 1 - k_\parallel, k_z)$ plane, taken with $h\nu = 440$–640 eV in steps of 2.5 eV. (e), (f) Spectra along the $(k_\parallel - 2, 1 - k_\parallel)$ direction with $k_z = 18$ (Z-A direction) and $k_z = 17$ (Γ-X direction), respectively. The superimposed dashed lines are the DFT bands renormalized by a factor $\sim$1.5.

Fe $3d$ band filling, i.e., the same strength of correlations in the $3d^{6.5}$ $LaRu_2P_2$ and $LaFe_2P_2$ and bigger $(W_{\mathrm{DFT}}/W)_{\mathrm{ARPES}}$ in $CaFe_2P_2$ and $BaFe_2As_2$, which are both nominally in the $3d^6$ configuration.

IV. DFT+DMFT DETAILS

The qualitative description above can be confirmed by theoretical calculations using the combined DFT+DMFT method which gives access to the spectral properties of these compounds. The DMFT calculations were performed in the implementation of Ref. [31], using the hybridization expansion continuous-time quantum Monte Carlo algorithm [32] as implemented in the TRIQS toolkit [33]. Localized Wannier orbitals were built by truncating the expansion of the initial atomiclike orbitals to an energy window $\mathcal{W}$, chosen here as $\mathcal{W} = [-7.5, 3]$ eV (see Ref. [31] for details). Calculations have been carried out at an inverse temperature of $\beta = 40\,\mathrm{eV}^{-1}$, in the paramagnetic phases of the compounds. The calculations of the Hubbard interactions and Hund's coupling (or more generally the Slater integrals F_0, F_2, F_4) have been performed using the constrained random phase approximation (cRPA) method in the implementation of Ref. [34].

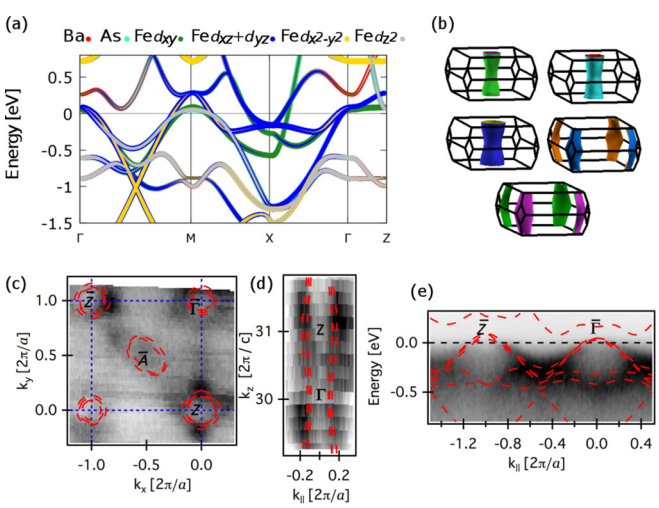

FIG. 4. (Color online) DFT band structure and SX-ARPES intensity maps of $BaFe_2As_2$. (a) Band structure along high symmetry lines. (b) Three-dimensional FS sheets of different bands. (c) FS map of $BaFe_2As_2$ with $h\nu = 840$ eV. (d) Intensity maps in the $(k_\parallel, 0, k_z)$ plane, taken with $h\nu = 720$–930 eV in steps of 10 eV. (e) Spectrum along the $(k_\parallel, 1)$ direction with $h\nu = 840$ eV ($k_z \sim 30$). The superimposed dashed lines are the DFT calculations renormalized by a factor $\sim$2.1.

V. DFT+DMFT RESULTS

The values obtained for the interactions are shown in Fig. 5(d). The DMFT spectral functions for the various samples are presented in Figs. 6(a)–6(d). The DFT band structures, overlaid on the respective spectral functions, are renormalized by a factor $(W_{\mathrm{DFT}}/W)_{\mathrm{DMFT}}$. The renormalized bands agree well with the DFT+DMFT spectral function at low binding energies, while they overestimate the correlation strength at higher binding energies, in agreement with our ARPES data. The resulting quasiparticle residues (denoted Z_{DMFT}) agree well with the Z_m values ($m = z^2, x^2 - y^2, xy, xz, yz$) directly extracted from the self-energy on the Matsubara

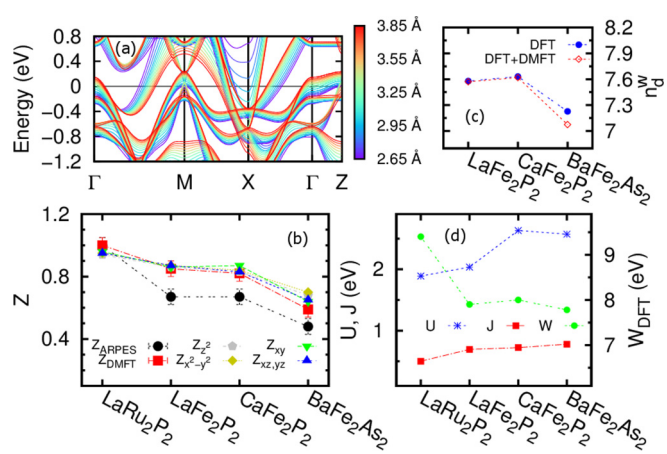

FIG. 5. (Color online) DFT and DFT+DMFT calculation results. (a) DFT calculation in $CaFe_2P_2$ as a function of the P-P distance. (b) Experimental and theoretical values of Z. (c) Orbital-dependent occupation of Wannier d orbitals within DFT and DFT+DMFT. (d) Calculated values of U_{cRPA}, J_{cRPA}, and W_{DFT}.

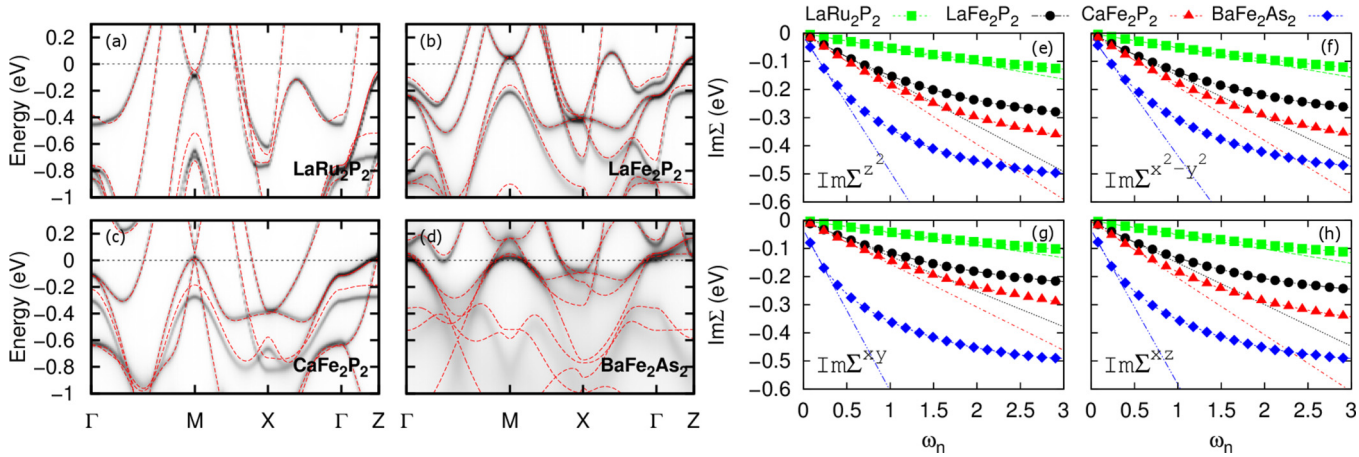

FIG. 6. (Color online) DFT+DMFT spectral functions and self-energies. (a)–(d) Spectral functions calculated with the DFT+DMFT method along high symmetry lines for $LaRu_2P_2$, $LaFe_2P_2$, $CaFe_2P_2$, and $BaFe_2As_2$, respectively. The DFT calculations superimposed are renormalized by the factors $(Z_{\mathrm{DMFT}})^{-1}$, with Z_{DMFT} displayed in Fig. 5(b). (e)–(h) Imaginary parts of the local many-body self-energy on the imaginary frequency axis.

grid as $Z_m = \{1 - \mathrm{Im}[\frac{d\Sigma_m(i\omega_n)}{d\omega_n}|_{\omega_n\to 0}]\}^{-1}$ [see Fig. 5(b)]. The calculated behavior agrees well with the experimental one; the correlations are negligible in $LaRu_2P_2$, increase in $LaFe_2P_2$, remain constant in $CaFe_2P_2$, and reach a maximum in $BaFe_2As_2$. Figures 6(e)–6(h) show the imaginary parts of the local many-body self-energy on the imaginary frequency axis, a quantity which in the Fermi liquid regime exhibits linear behavior at low energies (and a slope related to the quasiparticle residues as above). These curves show that the DMFT calculations display the trend of correlation strength for our series of compounds in two ways: Not only do the self-energies increase in overall value, with the steeper slopes for $BaFe_2As_2$ corresponding to the stronger quasiparticle renormalizations (smaller Z_m), but also the energetic *extent* of the linear regime decreases. In $BaFe_2As_2$, coherent quasiparticles exist only on very low-energy scales, while the other compounds display larger coherence scales. In the spectral functions, the signature of this effect is the overall quite substantial broadening observed in $BaFe_2As_2$, as compared to the other compounds. The small underestimation of (W_{DFT}/W) in the DMFT calculations as compared to experiment might be due to the local nature of the DMFT method [35] or the absence of dynamical screening in the calculations [7,36,37]. We also note that there is a sizable change in U_{cRPA} and J_{cRPA} only upon the Ru to Fe substitution and that, even in this case, it does not have a large influence on the correlations in our calculations. Indeed, the calculated Z_m for the $LaRu_2P_2$ are slightly changed by an increase in U_{cRPA} and J_{cRPA} (values obtained using the same U_{cRPA} and J_{cRPA} used for $BaFe_2As_2$ are $Z_{z^2} = 0.90$, $Z_{x^2-y^2} = 0.91$, $Z_{xy} = 0.92$, $Z_{xz,yz} = 0.90$). The evolution of the filling of the Wannier d orbitals, n_d^W, both before and after the DFT-DMFT calculations, is shown in Fig. 5(c). The filling of the orbitals is constant in $LaFe_2P_2$ and $CaFe_2P_2$ and decreases in $BaFe_2As_2$, in agreement with the qualitative conclusions drawn from the band structure calculations. We underline that the observed occupation-driven trend in the correlations confirms the link between cuprate and pnictide phase diagrams. In Ref. [1], a unified phase diagram for hole-doped cuprates and both hole- and electron-doped Fe-based pnictides was proposed by plotting T_c as a function of the nominal average orbital filling (y^{Nom}), expressed as the deviation from half filling of the Fe d bands (i.e., $n_{\mathrm{Fe}_d}^{\mathrm{Nom}} = 5 + 5y^{\mathrm{Nom}}$). To extend this picture in $LaFe_2P_2$ and $CaFe_2P_2$, we propose to use the Wannier orbital filling instead of the nominal value. We can calculate the average orbital filling with respect to the half-filled case for $i = LaFe_2P_2, CaFe_2P_2$ as $y_i = y_{\mathrm{BaFe_2As_2}}^{\mathrm{Nom}} + K \times (y_i^W - y_{\mathrm{BaFe_2As_2}}^W)$, with $y^W = (n_d^W - 5)/5$. The use of a linear relation between y^{Nom} and y^W, with $K \approx 1$, is supported by our DFT-virtual crystal approximation (VCA) calculations of y^W for $BaFe_{1-x}Co_xAs_2$. The resulting $y_{\mathrm{LaFe_2P_2}} = 0.27$ and $y_{\mathrm{CaFe_2P_2}} = 0.28$, obtained using n_d^W from our DFT calculations, places them in the overdoped nonsuperconducting side of the unified phase diagram proposed in Ref. [1]. At this doping the correlations are not strong enough to allow the development of unconventional superconductivity and to display differentiation of bandwidth renormalization, i.e., selective Mottness, for electrons with different band characters. These results are in agreement with our observation of moderated electronic correlations and absence of selective Mottness in $LaFe_2P_2$ and $CaFe_2P_2$.

We finally remark that a previous work has proposed $CaFe_2P_2$ as the structural analog of the collapsed tetragonal (CT) nonmagnetic phase of $CaFe_2As_2$ [26]. However, the measured correlation strength observed here for $CaFe_2P_2$ is smaller than the value reported for the CT phase of $CaFe_2As_2$ [38–40], indicating that there might be a fundamental difference between the two systems.

VI. CONCLUSION

In conclusion, we showed that the evolution of the electronic correlations in the presented series of pnictides differs from the expected behavior inferred from the nominal filling of the correlated orbitals. The experimental trend can be qualitatively understood based on the effective filling of the correlated orbitals and quantitatively reproduced by our DMFT calculations. We also demonstrated that the observed occupation-driven trend in the correlations supports the recently proposed link between the

unconventional superconductivity in cuprates and Fe pnictides. Finally, the high sensitivity of the correlations to small changes in the filling opens different ways of tuning the strength of electronic correlations in transition metal pnictide systems by systematic chemical substitutions, pressure, or constraints.

ACKNOWLEDGMENTS

This project was supported by the Swiss National Science Foundation (Grant No. 200021-137783), through MaNEP (Grant No. 200020-105151) and Division II, the French ANR under Project PNICTIDES, IDRIS/GENCI under Project No. 091393, the European Research Council under Project No. 617196, and the Cai Yuanpei program. P.R. and H.D. acknowledge grants from MOST (No. 2010CB923000, No. 2011CBA001000, No. 2011CB921701, No. 2013CB921700, and No. 2012CB821403) and NSFC (No. 11004232, No. 11234014, and No. 11274362) from China. The DFT+DMFT calculations were performed at DALCO cluster of the University of Fribourg. We thank Pawel Bednarek for support.

[1] L. de' Medici, G. Giovannetti, and M. Capone, Selective Mott Physics as a key to iron superconductors, Phys. Rev. Lett. **112**, 177001 (2014).

[2] Z. R. Ye, Y. Zhang, F. Chen, M. Xu, J. Jiang, X. H. Niu, C. H. P. Wen, L. Y. Xing, X. C. Wang, C. Q. Jin, B. P. Xie, and D. L. Feng, Extraordinary doping effects on quasiparticle scattering and bandwidth in iron-based superconductors, Phys. Rev. X **4**, 031041 (2014).

[3] T. Misawa, K. Nakamura, and M. Imada, *Ab Initio* evidence for strong correlation associated with mott proximity in iron-based superconductors, Phys. Rev. Lett. **108**, 177007 (2012).

[4] M. Aichhorn, S. Biermann, T. Miyake, A. Georges, and M. Imada, Theoretical evidence for strong correlations and incoherent metallic state in FeSe, Phys. Rev. B **82**, 064504 (2010).

[5] L. de' Medici, Hund's coupling and its key role in tuning multiorbital correlations, Phys. Rev. B **83**, 205112 (2011).

[6] K. Haule and G. Kotliar, Coherence-incoherence crossover in the normal state of iron oxypnictides and importance of Hund's rule coupling, New J. Phys. **11**, 025021 (2009).

[7] P. Werner, M. Casula, T. Miyake, F. Aryasetiawan, A. J. Millis, and S. Biermann, Satellites and large doping and temperature dependence of electronic properties in hole-doped $BaFe_2As_2$, Nat. Phys. **8**, 331 (2012).

[8] L. de' Medici, S. R. Hassan, M. Capone, and Xi Dai, Orbital-Selective mott transition out of band degeneracy lifting, Phys. Rev. Lett. **102**, 126401 (2009).

[9] A. Liebsch and H. Ishida, Correlation-induced spin freezing transition in FeSe: A dynamical mean field study, Phys. Rev. B **82**, 155106 (2010).

[10] N. Lanata, H. U. R. Strand, G. Giovannetti, B. Hellsing, L. de' Medici, and M. Capone, Orbital selectivity in Hund's metals: The iron chalcogenides, Phys. Rev. B **87**, 045122 (2013).

[11] N. Xu, P. Richard, A. van Roekeghem, P. Zhang, H. Miao, W.-L. Zhang, T. Qian, M. Ferrero, A. S. Sefat, S. Biermann, and H. Ding, Electronic Band Structure of $BaCo_2As_2$: A fully doped ferropnictide analog with reduced electronic correlations, Phys. Rev. X **3**, 011006 (2013).

[12] E. van Heumen, J. Vuorinen, K. Koepernik, F. Massee, Y. Huang, M. Shi, J. Klei, J. Goedkoop, M. Lindroos, J. van den Brink, and M. S. Golden, Existence, character, and origin of surface-related bands in the high temperature iron pnictide superconductor $BaFe_{2-x}Co_xAs_2$, Phys. Rev. Lett. **106**, 027002 (2011).

[13] E. Razzoli, M. Kobayashi, V. N. Strocov, B. Delley, Z. Bukowski, J. Karpinski, N. C. Plumb, M. Radovic, J. Chang, T. Schmitt, L. Patthey, J. Mesot, and M. Shi, Bulk electronic structure of superconducting $LaRu_2P_2$ single crystals measured by soft-X-ray angle-resolved photoemission spectroscopy, Phys. Rev. Lett. **108**, 257005 (2012).

[14] P. Richard, C. Capan, J. Ma, P. Zhang, N. Xu, T. Qian, J. D. Denlinger, G.-F. Chen, A. S. Sefat, Z. Fisk, and H. Ding, Angle-resolved photoemission spectroscopy observation of anomalous electronic states in $EuFe_2As_{2-x}P_x$, J. Phys.: Condens. Matter **26**, 035732 (2014).

[15] V. N. Strocov, X. Wang, M. Shi, M. Kobayashi, J. Krempasky, C. Hess, T. Schmitt, and L. Patthey, Soft-X-ray ARPES facility at the ADRESS beamline of the SLS: Concepts, technical realization and scientific applications, J. Synchrotron Radiat. **21**, 32 (2014).

[16] P. Blaha, K. Schwarz, G. K. H. Madsen, D. Kvasnicka, and J. Luitz, *WIEN2k, An Augmented Plane Wave + Local Orbitals Program for Calculating Crystal Properties* (Karlheinz Schwarz, Techn. Universität at Wien, Austria, 2001).

[17] A. Kokalj, Computer graphics and graphical user interfaces as tools in simulations of matter at the atomic scale, Comput. Mater. Sci. **28**, 155 (2003). Code available from http://www.xcrysden.org/.

[18] W. Jeitschko, R. Glaum, and L. Boonk, Superconducting $LaRu_2P_2$ and other alkaline earth and rare earth metal ruthenium and osmium phosphides and arsenides with $ThCr_2Si_2$ structure, J. Solid State Chem. **69**, 93 (1987).

[19] W. Jeitschko, U. Meisen, M. H. Möller, and M. Reehuis, Über $LaCo_2P_2$ und andere Neue Verbindungen mit $ThCr_2Si_2$- und $CaBe_2Ge_2$-Struktur, Z. Anorg. Allg. Chem. **527**, 73 (1985).

[20] A. Mewis, Ternäre Phosphide mit $ThCr_2Si_2$-Struktur, Z. Naturforsch. B **35**, 141 (1980).

[21] Q. Huang, Y. Qiu, W. Bao, M. A. Green, J. W. Lynn, Y. C. Gasparovic, T. Wu, G. Wu, and X. H. Chen, Neutron-diffraction measurements of magnetic order and a structural transition in the parent $BaFe_2As_2$ compound of FeAs-Based high-temperature superconductors, Phys. Rev. Lett. **101**, 257003 (2008).

[22] S. Hüfner, *Photoelectron Spectroscopy* (Springer, Berlin, 1995).

[23] The bandwidth renomalization factor is symbolically indicated as $(W_{\mathrm{DFT}}/W)_i$, with the index i (i = ARPES, DMFT) specifying whether it is obtained by rescaling the DFT bands to match the experimental spectral function or the calculated one. The associated quasiparticle residue Z is defined as $Z_i \equiv (W_{\mathrm{DFT}}/W)_i^{-1}$.

[24] P. Zhang, P. Richard, T. Qian, Y.-M. Xu, X. Dai, and H. Ding, A precise method for visualizing dispersive features in image plots, Rev. Sci. Instrum. **82**, 043712 (2011).

[25] P. J. W. Moll, J. Kanter, R. D. McDonald, F. Balakirev, P. Blaha, K. Schwarz, Z. Bukowski, N. D. Zhigadlo, S. Katrych,

K. Mattenberger, J. Karpinski, and B. Batlogg, Quantum oscillations of the superconductor $LaRu_2P_2$: Comparable mass enhancement $\lambda \approx 1$ in Ru and Fe phosphides, Phys. Rev. B **84**, 224507 (2011).

[26] A. I. Coldea, C. M. J. Andrew, J. G. Analytis, R. D. McDonald, A. F. Bangura, J.-H. Chu, I. R. Fisher, and A. Carrington, Topological change of the Fermi surface in ternary iron pnictides with reduced c/a Ratio: A de Haas–van Alphen Study of $CaFe_2P_2$, Phys. Rev. Lett. **103**, 026404 (2009).

[27] T. Terashima, N. Kurita, M. Tomita, K. Kihou, C.-H. Lee, Y. Tomioka, T. Ito, A. Iyo, H. Eisaki, T. Liang, M. Nakajima, S. Ishida, S.-I. Uchida, H. Harima, and S. Uji, Complete fermi surface in $BaFe_2As_2$ observed via shubnikov–de Haas Oscillation measurements on detwinned single crystals, Phys. Rev. Lett. **107**, 176402 (2011).

[28] H. Ishida and A. Liebsch, Fermi-liquid, non-Fermi-liquid, and Mott phases in iron pnictides and cuprates, Phys. Rev. B **81**, 054513 (2010).

[29] P. Richard, T. Sato, K. Nakayama, T. Takahashi, and H. Ding, Fe-based superconductors: An angle-resolved photoemission spectroscopy perspective, Rep. Prog. Phys. **74**, 124512 (2011).

[30] O. K. Andersen, and L. Boeri, On the multi-orbital band structure and itinerant magnetism of iron-based superconductors, Ann. Phys. **1**, 8 (2011).

[31] M. Aichhorn, L. Pourovskii, V. Vildosola, M. Ferrero, O. Parcollet, T. Miyake, A. Georges, and S. Biermann, Dynamical mean-field theory within an augmented plane-wave framework: Assessing electronic correlations in the iron pnictide LaFeAsO, Phys. Rev. B **80**, 085101 (2009).

[32] P. Werner, A. Comanac, L. de' Medici, M. Troyer, and A. J. Millis, Continuous-time solver for quantum impurity models, Phys. Rev. Lett. **97**, 076405 (2006).

[33] M. Ferrero and O. Parcollet, Continuous-time solver for quantum impurity models TRIQS: A Toolbox for Research on Interacting Quantum Systems, http://ipht.cea.fr/triqs.

[34] L. Vaugier, H. Jiang, and S. Biermann, Hubbard U and Hund exchange J in transition metal oxides: Screening versus localization trends from constrained random phase approximation, Phys. Rev. B **86**, 165105 (2012).

[35] A. Georges, G. Kotliar, K. Werner, and M. J. Rozenberg, Dynamical mean-field theory of strongly correlated fermion systems and the limit of infinite dimensions, Rev. Mod. Phys. **68**, 13 (1996).

[36] M. Casula, P. Werner, L. Vaugier, F. Aryasetiawan, T. Miyake, A. J. Millis, and S. Biermann, Low-energy models for correlated materials: Bandwidth renormalization from coulombic screening, Phys. Rev. Lett. **109**, 126408 (2012).

[37] A. van Roekeghem, T. Ayral, J. M. Tomczak, M. Casula, N. Xu, H. Ding, M. Ferrero, O. Parcollet, H. Jiang, and S. Biermann, Dynamical correlations and screened exchange on the experimental bench: Spectral properties of the cobalt pnictide $BaCo_2As_2$, Phys. Rev. Lett. **113**, 266403 (2014).

[38] K. Gofryk, B. Saparov, T. Durakiewicz, A. Chikina, S. Danzenbächer, D. V. Vyalikh, M. J. Graf, and A. S. Sefat, Fermi-surface reconstruction and complex phase equilibria in $CaFe_2As_2$, Phys. Rev. Lett. **112**, 186401 (2014).

[39] J. Diehl, S. Backes, D. Guterding, H. O. Jeschke, and R. Valentí, Correlation effects in the tetragonal and collapsed-tetragonal phase of $CaFe_2As_2$, Phys. Rev. B **90**, 085110 (2014).

[40] S. Mandal, R. E. Cohen, and K. Haule, Pressure suppression of electron correlation in the collapsed tetragonal phase of $CaFe_2As_2$: A DFT-DMFT investigation, Phys. Rev. B **90**, 060501(R) (2014).